






Curve Negotiation Characteristics of the Side-Suspended High-Temperature Superconducting Maglev System

Zongpeng Li^{1,2} , Li Wang^{1,2} , Xiaofei Wang^{1,2} , Zigang Deng^{2*} 

¹ School of Mechanics and Aerospace Engineering, Southwest Jiaotong University, 610031 Chengdu, China

² State Key Laboratory of Traction Power, Southwest Jiaotong University, 610031 Chengdu, China

* Correspondence: Zigang Deng (deng@swjtu.cn)

Received: 08-11-2022

Revised: 09-13-2022

Accepted: 09-21-2022

Citation: Z. P. Li, L. Wang, X. F. Wang, and Z. G. Deng, "Curve negotiation characteristics of the side-suspended high-temperature superconducting maglev system," *Mechatron. Intell Transp. Syst.*, vol. 1, no. 1, pp. 47-56, 2022. <https://doi.org/10.56578/mits010106>.



© 2022 by the authors. Licensee Acadlore Publishing Services Limited, Hong Kong. This article can be downloaded for free, and reused and quoted with a citation of the original published version, under the CC BY 4.0 license.

Abstract: Thanks to its superb curve negotiation characteristics, the side-suspended high-temperature superconducting (SS-HTS) maglev system boasts a great potential for high-speed transportation. The SS-HTS maglev system, however, significantly differs in suspension features from the conventional maglev system because of its unique side-suspended structure. To improve suspension performance, the field-cooling technique of superconducting bulks in the SS-HTS system was investigated through a number of experiments. To fit the experimental data, the authors proposed the mathematical models of the levitation and guidance forces as well as the optimal field-cooling position. Furthermore, a dynamic model was developed for the SS-HTS maglev vehicle operating on a curve line, and the curve negotiation characteristics were simulated for the maglev vehicle. Finally, the stability of the curve negotiation for the SS-HTS system was assessed using the Sperling index. The results show that the SS-HTS maglev vehicle can pass over bends at a certain speed. The authors also recommended the suspension parameters the maglev vehicle.

Keywords: Side-suspended high-temperature superconducting (SS-HTS) maglev system; Vehicle dynamics; Field-cooling method; Curve negotiation

1. Introduction

High-temperature superconducting (HTS) levitation systems are capable of maintaining stable levitation without the need for intricate controls, thanks to the flux-pinning property of HTS bulk materials [1-3]. The HTS maglev has advantages over electromagnetic suspension (EMS) and electrodynamic suspension (EDS), including self-stability, low energy consumption, low operating costs, etc. In 2016, a n SS-HTS maglev train model system was created by the Superconducting and New Energy Research and Development Center, Southwest Jiaotong University [4-6]. The system was thoroughly detailed by Zhou et al. [7] and Liu et al. [8].

Compared to the general type, in the SS-HTS system, the permanent magnet guideway (PMG) and superconducting bulks are rotated 90 degrees [9-12], the guidance force overcomes gravity, and the levitation force provides the centripetal force when the curve passes. The system has a higher curve-passing performance than the general type, for the levitation force is typically greater than the guidance force and can alter with the levitation gap. Currently, circular systems are where the SS-HTS maglev vehicles are most frequently deployed.

Numerous scholars worked on the suspension properties of HTS bulks in the prior studies. For example, Ren et al. [13] investigated the impacts of field-cooling position, superconductor size, and combination method on the suspension features of the system. Navau et al. [14] studied the levitation equilibrium position of superconductors during different field-cooling processes. Focusing on the side-suspended system, Zhou et al. [7] derived the analytical solutions of the guidance force and the levitation force of the SS-HTS maglev system. Liu et al. [8] used finite-element simulation (FEM) software to establish a three-dimensional FEM model for the side-suspended system, and identified the coupling features of two superconducting bulks.

Meanwhile, many researchers from the Southwest Jiaotong University have probed into the HTS maglev dynamics. For instance, Deng et al. [15] established modeled the dynamics of an HTS maglev train with 11 degrees

of freedom (DOFs). The model includes a vehicle body and two levitation bogies. Next, they studied the free vibration of the maglev train. Deng et al. [15] established a vertical vehicle-bridge coupled dynamics system, in the light of the disturbance of the track irregularity. Wang et al. [16] set up a three-vehicle six-levitation bogies model based on the UM software, simulated the vehicle-bridge coupling dynamics, and examined the vertical vibration response. Using the UM software, Ma et al. [17] set up a vehicle-bridge coupling dynamic model under curve passing, and measured the influence of vehicle parameters on vehicle vibration.

Since most engineering applications of the SS-HTS system is still in the laboratory stage, this paper carries out additional research beginning with the dynamic features of the bulks, simulating the high-speed running condition, and offering recommendations for future applications. In this study, the ideal position in the field-cooling process is investigated along with its laws, and a dynamic analysis is performed afterwards. The objective is to evaluate how well the SS-HTS maglev system negotiates curves and to serve as a reference for further investigation.

2. Methodology

2.1 Experimental Setup

Monopole and two-pole PMGs are the two main types of PMGs at the moment [18]. The ring test line "Super-Maglev" incorporates two-pole PMGs, while the first man-loading HTS maglev, "Century," uses monopole PMGs [4]. The two-pole PMGs were adopted in our experiments. Figure 1 roughly depicts their structure, size, and magnetization direction. The x-axis direction is defined as the direction of lateral displacement, and the z-axis direction as the vertical direction. This coordinate system is applied consistently throughout the following research.

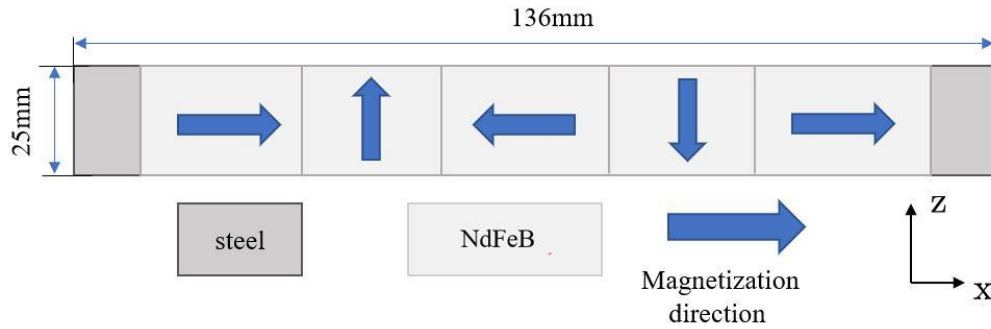
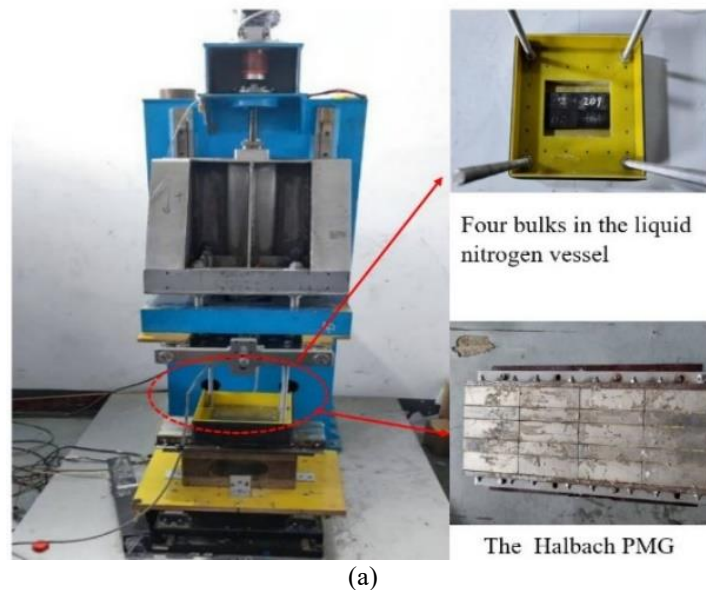


Figure 1. Structure, dimension, and magnetization direction of the PMG

The experiments were carried out on a self-developed HTS maglev test system, SCML-01 [12]. There were four rectangular superconducting bulks. The length, width, and thickness of each bulk are 64 mm, 32 mm, and 12 mm, respectively. Subgraph (a) of Figure 2 presents an actual image of the device.



(a)

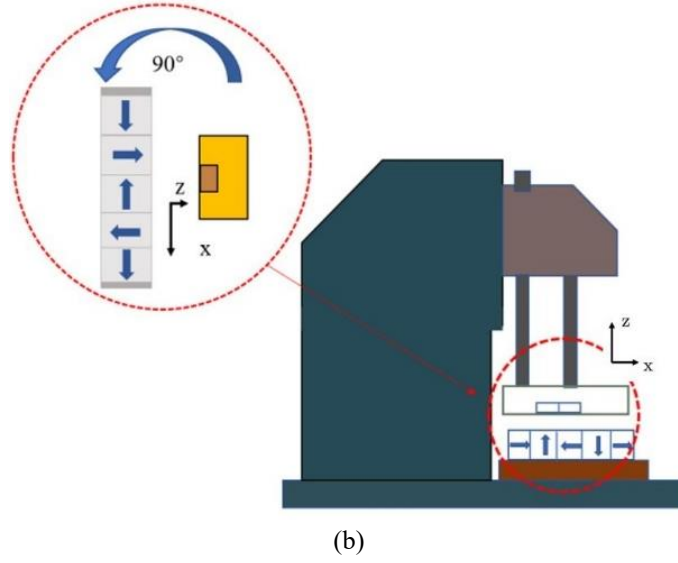


Figure 2. Measuring device for the guidance force of the HTS bulks (a) SCML-01, (b) Bulks placement

During the experiments, the entire side-suspended system of SCML-01 and the corresponding coordinate system were rotated 90 degrees counterclockwise. Figure 2 shows the structure of the experimental device and illustrates the bulks placement. This system of the device mainly measures the guidance force and levitation force of the SS-HTS system.

2.2 Experimental Principle

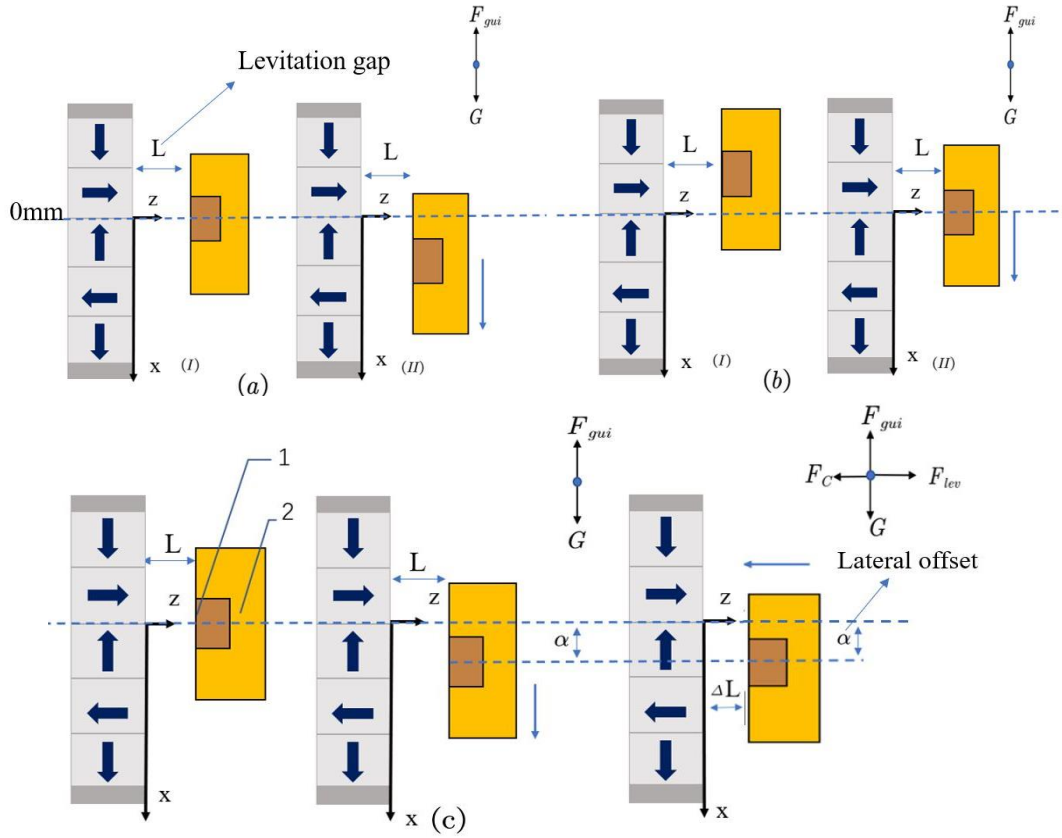


Figure 3. The three field-cooling methods. (a) Field-cooling initial position at the lateral displacement of 0 mm; (b) Field cooling initial position over 0mm; (c) Changing levitation gap ΔL during field-cooling; 1-HTS bulks, 2-liquid nitrogen vessel

From the field-cooling of the superconducting bulks to the operation of the maglev vehicle, there will be a series of changes in the position and stress state of the bulks. We reference Liu's research [8] and divide it into three processes: (a) The superconducting bulk is located in the center of the PMG to start field-cooling; (b) Due to gravity G , the bulk displaces downward and begins to be subjected to the guidance force F_{gui} ; (c) When passing curve, due to centrifugal force F_C , the bulk is close to the PMG and is subjected to the levitation force F_{lev} . Considering the distribution of magnetic field lines around the PMG [19], and the aforementioned three processes, we define three methods of field-cooling, as shown in Figure 3. The dotted line in Figure 3 is at the specified lateral displacement of 0 mm, and the levitation gap at the beginning of field-cooling is the field-cooling height.

To study the aforementioned process, we designed two experiments to simulate the process and explore the optimal field-cooling position. Case 1: Studying the Field-cooling method (a) and (b). Starting field-cooling at different positions, studying the variation law of the guidance force, and finding the optimal lateral field-cooling position during this motion. Case 2: Studying the Field-cooling method (c), simulating the process. Start the field-cooling in the optimal lateral field-cooling position obtained in Case 1, first move a distance along the direction of gravity (x-axis direction), then gradually approach the PMG. To expand and contract in the same direction, record the guidance force data during this process, find the optimal field-cooling position during this movement and compare it with the results of case 1.

In the side-suspended system, the guidance force reflects the vertical stability of the system, so the criterion for the optimal field-cooling position is the position where the maximum guidance force occurs. Based on the experimental principle, two experimental schemes were designed, with a total of five groups (A, B, C, D, and E). The experimental groups are shown in Table 1.

Table 1. Experimental parameter setting of A, B, C, and D group

Group	Initial field-cooling position (x, z) mm	Range of motion	Movement direction
A	(0, 10)	0~40 mm	lateral
B	(-10, 10)	-10~40 mm	lateral
C	(-20, 10)	-20~40 mm	lateral
D	(-30, 10)	-30~40 mm	lateral

As shown in Table 1, the initial field-cooling position (x, z), x represents the lateral offset position, and z refers to the field-cooling height. Among them, the initial lateral offset position of the B, C, and D group is the position of the maximum guidance force in the previous group. For Case 1, we performed four sets of A, B, C, and D groups in turn, with the field-cooling height unchanged, to gradually explore the effect of the lateral offset position on the magnitude of the guidance force. For Case 2, we simulate case 2 by changing the suspension gap with the result in case 1 as the initial lateral position. In the E group, according to the experimental experience [7, 8], the change range of the levitation gap is set to the range of 2~10 mm, to explore the comparison between the field-cooling method (c) and the former, then obtain the optimal field-cooling position.

3. Simulation Model

Next, we plan to apply the experimental results to the simulation of the SS-HTS system. The simulation method can effectively study the curve negotiation characteristics of the system at high speed, and at the same time, the influence of different parameters can be studied. A widely used railway simulation software Universal mechanism (UM) was used to develop the model of the SS-HTS maglev system. Many researchers have conducted a lot of meaningful simulation analyses in the field of rail transit by UM software [20-22], and these simulation data are in good agreement with the measured data. These experiences indicate the reliability of UM for the SS-HTS system simulation analyses. Referring to the parameters from the experimental prototype [14-19], an SS-HTS maglev vehicle model was built, which consists of 3 vehicles, and each vehicle includes 2 suspension bogies. In the structure of the SS-HTS maglev train, the liquid nitrogen vessels with superconducting bulks are installed on both sides of the suspension bogie, and the PMGs are also installed on both sides to achieve the effect of side-suspended so that the guidance force overcomes gravity, and the levitation force provides the centripetal force. There are 24 liquid nitrogen vessels in each suspension bogie. A rigid vehicle body is supported by 4 air springs. Figure 4 shows the model of the maglev train in UM.

In future engineering applications, HTS maglev vehicles are more likely to be used on elevated rail bridges. The track bridge was modeled through the flexible track beam bridge module that comes with UM software. In the vehicle system, the secondary suspension system plays the role of supporting the vehicle body, alleviating the impact and the vibration, which is a key factor to improve the dynamic performance of the vehicle. And the stability of the vehicle is also important. So, we plan to study the dynamic response of the vehicle to make recommendations for the secondary series suspension parameters and to evaluate the curved negotiating stability of the SS-HTS maglev vehicle.

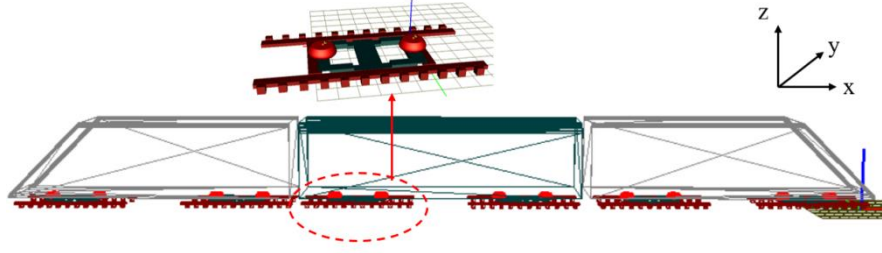


Figure 4. The SS-HTS maglev train model in UM, the liquid nitrogen vessels with superconducting bulks are installed on both sides

4. Results and Discussion

4.1 The Optimal Field-Cooling Position

The A, B, C, and D groups data of case 1 are shown in Figure 5, and the position of the maximum value of the guidance force is gradually explored in Table 2.

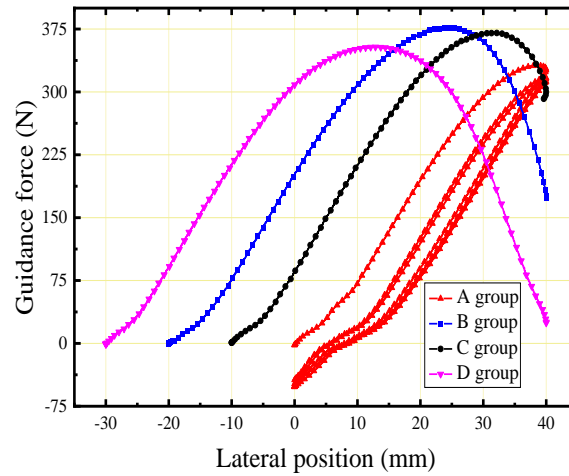


Figure 5. Guidance force curves of the HTS bulks at the chosen lateral displacement ranges of 0-40, -10-40, -20-40, and -30-40 mm

Table 2. The maximum guidance force and position of the A, B, C, and D group

Group	Maximum guidance force (N)	Lateral position (mm)
A	324.4	35.2
B	376.0	25.3
C	370.3	31.2
D	353.5	12.7

It is observed that the guidance force increases with the increasing distance away from the equilibrium position. However, when the distance exceeds a certain range, the guidance force begins to decrease. And the maximum guidance force of group A appeared at the lateral position of 35 mm, so we carried out the next group of experiments based on this. According to experience, there is a safety margin of 15 mm, so the initial position of the group B experiment is set to 20 mm. According to the above method, the experiments of group C and group D were carried out in turn. Meanwhile, a maximum value of guidance force appears in each group of data, and the maximum value of group B exceeds that of the other three groups.

It can be seen from Table 2 that the maximum value of the guidance force is 376.0 N in the B group experiment, and the appearance position is 25.3 mm. Therefore, we take this as the current optimal lateral field-cooling position and then conduct Case 2. In Case 2, group E was carried out with 10 mm as the initial field-cooling height and -20 mm as the initial lateral field-cooling position, and the data of the change of the guidance force with the lateral position was extracted as shown in Figure 6. The maximum value of the guidance force in Figure 6 is 490.7 N,

which is greater than all the data in case 1. The maximum value of the guidance force appears at the position of 28.5 mm, and we also leave a safety margin of 15 mm, so it can be concluded that the optimal lateral field cooling position is 13.5 mm. The reason for this is analyzed, indicating that the bulk is cooled at a position above the magnetic peak, and better performance can be obtained due to gravity falling to the peak position.

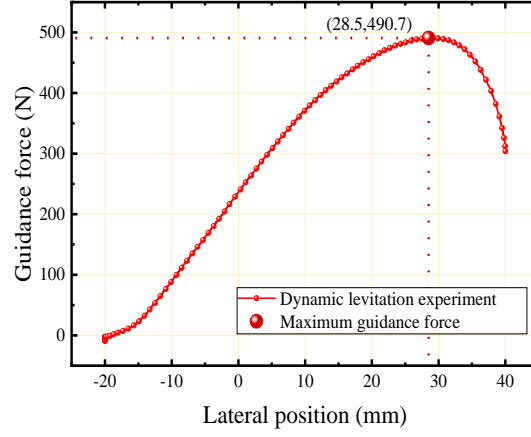


Figure 6. Group E, guidance force curves of the HTS bulks at the chosen lateral displacement ranges of -20-40 mm

4.2 The Levitation and Guidance Force

The experiments were carried out at the optimal field-cooling position to fit the data of the levitation force and the guidance force. Considering comprehensively, we selected the single-exponential model and double-exponential models for fitting. For the guidance force, the curve has a good linear trend, which can be equivalent to the spring model of Hooke's law. Ignoring the hysteresis characteristics, only the data of the ascending section of the levitation force is used for fitting. And the fitting result of the levitation and guidance force is shown in Figure 7.

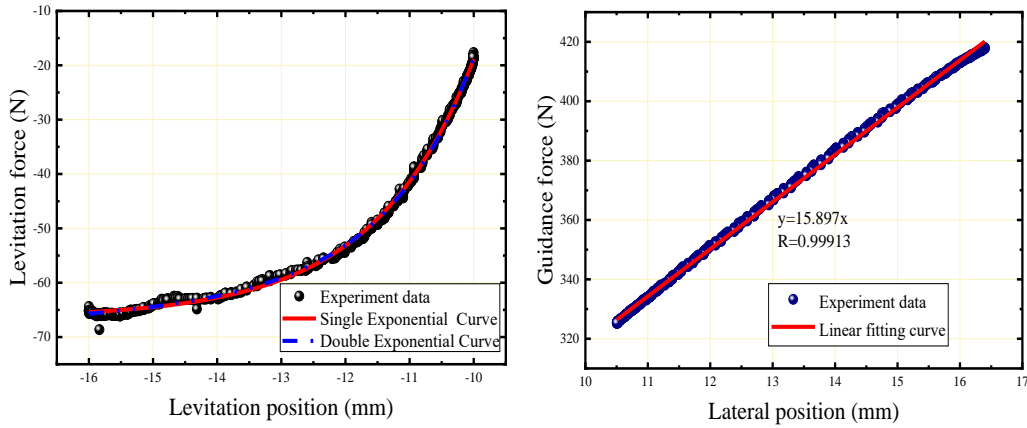


Figure 7. Levitation force and guidance force fitting curve

Single exponential formula and confidence:

$$y = 28451.150e^{\left(\frac{1}{1.564}x\right)} - 66.4315, R^2 = 0.998 \quad (1)$$

Double exponential formula and confidence:

$$y = 86978.373e^{\left(\frac{1}{1.29}x\right)} + 141.408e^{\left(\frac{1}{4.212}x\right)} - 69.223, R^2 = 0.999 \quad (2)$$

Observing Figure 7, it can be seen that the fitting effect of the three models is all good. Considering Eq. (2) of the model is obtained by integrating the double exponential form of Halbach's magnetic field strength, which has better rationality [16]. Linear fitting of the guidance force data is used, and the fitting degree is above 0.999, indicating that the fitting effect is good. Therefore, the fitting result of the double-exponential and linear formula is selected as the levitation and guidance force model in this paper. During the simulation, to achieve the suspension characteristics of the SS-HTS system, we set the guidance force to overcome gravity in the vertical direction and the levitation force to provide the centripetal force when passing the curve, through the custom module of the UM. In the custom module, we use the levitation and guiding force formulas obtained from the experiments for simulation:

$$F_{\text{lev}} = 86978.373e^{\left(\frac{1}{1.29}z\right)} + 141.408e^{\left(\frac{1}{4.212}z\right)} - 69.223 \quad (3)$$

$$F_{\text{gui}} = 15.897x \quad (4)$$

where, x and z refer to the lateral offset and the levitation gap, respectively.

4.3 Simulation Calculation Results

When establishing the SS-HTS system, we have always simplified the secondary suspension into a spring-damping system, we mainly study the effects of vertical stiffness and lateral stiffness on the dynamic response of the vehicle system. Referring to Ma's research [17], we selected the rear levitation bogie of the tail vehicle as the research object. According to the existing research [17, 19], the curve of radius R at the speed v and the superelevation angle have a great influence on the stability of the HTS maglev train. So, the simulation content is set as follows: When the vertical/lateral stiffness is 50 kN/m, 100 kN/m, 200 kN/m, 400 kN/m, and 500 kN/m, on a curved line with a radius of 8,000 m and a superelevation angle of 5° , the distance is 300 km. The dynamic response of the system when running at a speed of 300 km/h.

We selected the six most concerning dynamic indicators [19] in the simulation process:

- A: the amplitude of lateral acceleration of the vehicle body;
- B: the amplitude of vertical acceleration of the vehicle body;
- C: the amplitude of the lateral offset of the liquid nitrogen vessel;
- D: Lateral displacement amplitude of vehicle body;
- E: The fluctuation amplitude of the levitation gap;
- F: Vertical displacement amplitude of vehicle body; to measure the effect of parameter changes on the dynamic response of the system.

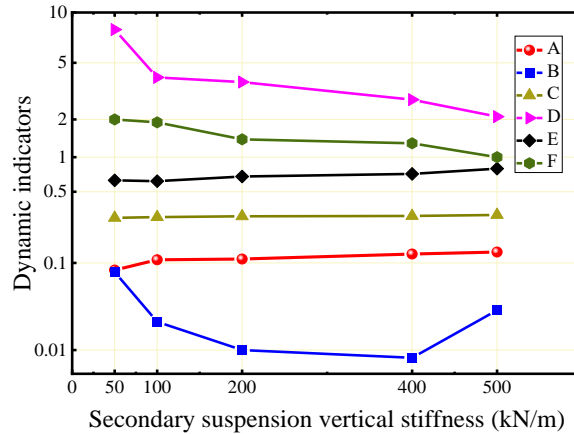


Figure 8. Influence of the vertical suspension stiffness of the suspension system on the running stationarity of the vehicle, under running the liquid nitrogen vessels with superconducting bulks are installed on both sides

It can be seen from Figure 8 that with the increase of the vertical stiffness, the amplitude of the lateral and vertical vibration acceleration of the vehicle body will increase, to affect the running stability of the vehicle, but too small vertical stiffness will cause too large lateral displacement to affect the safety of vehicle operation. Therefore, it is considered to choose the vertical stiffness of 100 kN/m, which is within this range, the dynamic indicators are relatively safe, and the fluctuation range of the suspension gap is the most stable, as the best vertical

stiffness parameter of the secondary suspension. According to the same way, the influence of lateral stiffness is analyzed, and the recommended value of the optimal lateral stiffness parameter is 100 kN/m. Finally, we use the Sperling stability index to evaluate the stability of the SS-HTS maglev train passing through the curved line at a speed of 300~800 km/h by calculation. The final calculated W parameter can be compared to Table 3 to obtain the evaluation of vehicle body stability. Extract the required calculation parameters in the UM software and use the Sperling statistical function. The calculation results are shown in Table 4.

Table 3. Vehicle stability rating table

Stationarity level	Assessment	Spring index
1	Excellent	$W < 2.5$
2	Good	$2.5 < W < 2.75$
3	Qualified	$2.75 < W < 3.0$

Table 4. Sperling index of vehicles at different running speeds

Vehicle velocity (km/h)	300	400	500	600
Vertical Stationarity Index	1.7602	1.892	2.282	2.356
Lateral Stationarity Index	1.599	1.845	1.899	2.009

According to the calculation results, the horizontal and vertical stability indexes of the vehicles are all less than 2.5 at different running speeds, and the evaluation level is “excellent”. Further analysis shows that with the increase of the running speed, the horizontal and vertical stability index of the car body also increases, the stability decreases, and the vertical stability index of the car body is slightly larger than the lateral stability index, which also shows that the excellent curve passing performance of the side-mounted HTS maglev vehicle system.

5. Conclusions

To summarize, for the maglev structure, the magnitude of the guidance force is related to the filed-cooling method, so we designed five groups of experiments to explore the optimal field-cooling methods of the SS-HTS system. and finally obtained the optimal field-cooling position (field-cooling height of 10 mm, lateral field-cooling position of 13.5 mm) and fitted good levitation force and guidance force equations.

Aiming to analyze the curve negotiation characteristics of the SS-HTS maglev system, a simulation model of the SS-HTS maglev train with three vehicles running on flexible tracks was established in UM. In terms of simulation calculation results, the 100 N/m vertical stiffness parameters and the 100 N/m lateral stiffness are suggested to design the suspension system of the SS-HTS maglev vehicle, which will enable it to have the ability to pass through a curve with a radius of 8000 m at the speed of 300 km/h safely and stationary. Then, the Sperling index was used to evaluate its running stability. The results show that in the case of the simple curve passing without adding line irregularity excitation, under the operating speed of 300 ~ 600 km/h, the vehicle's lateral and vertical stability ratings have reached "excellent", and the lateral stability is slightly higher than the vertical stability, indicating that the SS-HTS maglev vehicle has excellent curve passing ability. Overall, the results could be a reference for the SS-HTS system and lay a foundation for the subsequent updating and research of the future application of high-speed maglev train technology.

Funding

This work was partially supported by the National Natural Science Foundation of China (52022086); the Sichuan Science and Technology Program (22CXTD0070); and the Fundamental Research Funds for the Central Universities (2682022ZT051).

Data Availability

The data used to support the research findings are available from the corresponding author upon request.

Conflicts of Interest

The authors declare no conflict of interest.

References

- [1] E. H. Brandt, “Levitation in physics,” *Science*, vol. 243, no. 4889, pp. 349-355, 1989.

- <https://doi.org/10.1126/science.243.4889.349>.
- [2] F. C. Moon, *Superconducting Levitation: Applications to Bearings and Magnetic Transportation*, Hoboken NJ, USA: John Wiley & Sons, 1994.
 - [3] H. W. Lee, K. C. Kim, and J. Lee, "Review of maglev train technologies," *IEEE Trans. Mag.*, vol. 42, no. 7, pp. 1917-1925, 2006. <https://doi.org/10.1109/TMAG.2006.875842>.
 - [4] Z. Deng, W. Zhang, J. Zheng, B. Wang, Y. Ren, X. Zheng, and J. Zhang, "A high-temperature superconducting maglev-evacuated tube transport (HTS Maglev-ETT) test system," *IEEE Trans. Appl. Supercond.*, vol. 27, no. 6, pp. 1-8, 2017. <https://doi.org/10.1109/TASC.2017.2716842>.
 - [5] L. Schultz, O. de Haas, P. Verges, C. Beyer, S. Rohlig, H. Olsen, L. Kuhn, D. Berger, U. Noteboom, and U. Funk, "Superconductivity levitated transport system-the Supra Trans project," *IEEE Trans. Appl. Supercond.*, vol. 15, no. 2, pp. 2301-2305, 2005. <https://doi.org/10.1109/TASC.2005.849636>.
 - [6] F. N. Werfel, U. Floegel-Delor, R. Rothfeld, T. Riedel, P. Schirrmeister, and R. Koenig, "Experiments of superconducting maglev ground transportation," *IEEE Trans. Appl. Supercond.*, vol. 26, no. 3, pp. 1-5, 2016. <https://doi.org/10.1109/TASC.2016.2524471>.
 - [7] D. Zhou, C. Cui, L. Zhao, Y. Zhang, X. Wang, and Y. Zhao, "Static and dynamic stability of the guidance force in a side-suspended HTS maglev system," *Supercond Sci. Tech.*, vol. 30, no. 2, 2017. <https://doi.org/10.1088/1361-6668/30/2/025019>.
 - [8] J. Liu, F. Cai, D. Zhou, L. Zhao, Y. Zhang, and Y. Zhao, "Study of numerical simulation and dynamic performance optimization in evacuated tube SS-HTS maglev loop system," *Physica C: Supercond. Its Appl.*, vol. 565, Article ID: 1253504, 2019. <https://doi.org/10.1016/j.physc.2019.06.007>.
 - [9] J. S. Wang, S. Wang, Y. Zeng, H. Huang, F. Luo, Z. Xu, Q. Tang, G. Lin, C. Zhang, Z. Ren, G. Zhao, D. Zhu, S. Wang, H. Jiang, M. Zhu, C. Deng, P. Hu, C. Li, F. Liu, J. Lian, X. Wang, L. Wang, X. Shen, and X. Dong, "The first man-loading high-temperature superconducting maglev test vehicle in the world," *Physica C: Supercond.*, vol. 378, no. 1, pp. 809-814, 2002. [http://dx.doi.org/10.1016/S0921-4534\(02\)01548-4](http://dx.doi.org/10.1016/S0921-4534(02)01548-4).
 - [10] G. G. Sotelo, R. A. H. de Oliveira, F. S. Costa, D. H. N. Dias, R. de Andrade, and R. M. Stephan, "A full scale superconducting magnetic levitation (MagLev) vehicle operational line," *IEEE Trans. Appl. Supercond.*, vol. 25, no. 3, pp. 1-5, 2015. <https://doi.org/10.1109/TASC.2014.2371432>.
 - [11] Z. G. Deng, W. Zhang, J. Zheng, and Y. Ren, "A high-temperature superconducting maglev ring test line developed in Chengdu, China," *IEEE Trans. Appl. Supercond.*, vol. 26, no. 6, pp. 1-1, 2016. <http://dx.doi.org/10.1109/TASC.2016.2555921>.
 - [12] Z. G. Deng, J. Li, W. Zhang, Y. Gou, Y. Ren, and J. Zheng, "High-temperature superconducting magnetic levitation vehicles: Dynamic characteristics while running on a ring test line," *IEEE Veh. Technol. Mag.*, vol. 12, no. 3, pp. 95-102, 2017. <https://doi.org/10.1109/MVT.2017.2700493>.
 - [13] Z. Y. Ren, J. Wang, S. Wang, H. Jiang, M. Zhu, X. Wang, and H. Song, "Influence of shape and thickness on the levitation force of YBaCuO bulk HTS over a NdFeB guideway," *Physica C: Supercond.*, vol. 384, no. 1-2, pp. 159-162, 2003. [https://doi.org/10.1016/S0921-4534\(02\)01803-8](https://doi.org/10.1016/S0921-4534(02)01803-8).
 - [14] C. Navau, A. Sanchez, E. Pardo, and D. X. Chen, "Equilibrium positions due to different cooling processes in superconducting levitation systems," *Supercond Sci. Tech.*, vol. 17, no. 7, pp. 828-828, 2004. <http://dx.doi.org/10.1088/0953-2048/17/7/002>.
 - [15] Z. Deng, J. Li, H. Wang, Y. Li, and J. Zheng, "Dynamic simulation of the vehicle/bridge coupled system in high-temperature superconducting Maglev," *Comput. Sci. Eng.*, vol. 21, no. 3, pp. 60-71, 2019. <https://doi.org/10.1109/MCSE.2019.2902452>.
 - [16] H. Wang, Z. Deng, S. Ma, R. Sun, H. Li, and J. Li, "Dynamic simulation of the HTS maglev vehicle-bridge coupled system based on levitation force experiment," *IEEE Trans. Appl. Supercond.*, vol. 29, no. 5, pp. 1-6, 2019. <https://doi.org/10.1109/TASC.2019.2895503>.
 - [17] S. S. Ma, Z. Deng, H. Li, J. Yu, W. Zhang, Y. Hong, and J. Zheng, "Levitation height drifts of HTS bulks under a long-term external disturbance," *J. Supercond. Nov Magn.*, vol. 32, no. 12, pp. 3803-3810, 2019. <https://doi.org/10.1007/s10948-019-05170-0>.
 - [18] J. S. Wang, S. Y. Wang, Z. Y. Ren, M. Zhu, H. Jiang, and Q. X. Tang, "Levitation force of a YBaCuO bulk high-temperature superconductor over a NdFeB guideway," *IEEE Trans. Appl. Supercond.*, vol. 11, no. 1, pp. 1801-1804, 2001. <http://dx.doi.org/10.1109/77.920136>.
 - [19] H. T. Li, Z. Deng, Z. Ke, J. Yu, S. Ma, and J. Zheng, "Curve negotiation performance of high-temperature superconducting maglev based on guidance force experiments and dynamic simulations," *IEEE Trans. Appl. Supercond.*, vol. 30, no. 1, pp. 1-11, 2020. <https://doi.org/10.1109/TASC.2019.2932283>.
 - [20] Q. Wu, M. Spiriyagin, C. Cole, C. Chang, G. Guo, A. Sakalo, W. Wei, X. Zhao, N. Burgelman, P. Wiersma, H. Chollet, M. Sebes, A. Shamdani, S. Melzi, F. Cheli, E. Gialleonardo, N. Bosso, N. Zampieri, S. Luo, H. Wu, and G. Kaza, "International benchmarking of longitudinal train dynamics simulators: Results," *Veh. Syst. Dyn.*, vol. 56, no. 3, pp. 343-365, 2018. <https://doi.org/10.1080/00423114.2017.1377840>.
 - [21] R. Kovalev, A. Sakalo, V. Yazykov, A. Shamdani, R. Bowey, and C. Wakeling, "Simulation of longitudinal dynamics of a freight train operating through a car dumper," *Veh. Syst. Dyn.*, vol. 54, no. 6, pp. 707-722, 2016.

<https://doi.org/10.1080/00423114.2016.1153115>.

- [22] H. Jing, J. Wang, S. Wang, L. Wang, L. Liu, J. Zheng, Z., Deng, G. Ma, Y. Zhang, and J. Li, "A two-pole Halbach permanent magnet guideway for the high-temperature superconducting maglev vehicle," *Physica C: Supercond. Its Appl.*, vol. 463, pp. 426-430, 2007. <https://doi.org/10.1016/j.physc.2007.05.030>.